Journal Name

ARTICLE

Synthetic, Structural and Magnetic Implications of Introducing 2,2'-Dipyridylamide to Sodium-Ferrate Complexes

Received 00th January 20xx,
Accepted 00th January 20xx

DOI: 10.1039/x0xx00000x

www.rsc.org/

Lewis C. H. Maddock,[a] Ivana Borilovic,[b] Jamie McIntyre,[a] Alan R. Kennedy,[a] Guillem Aromí*[b] and Eva Hevia*[a]

Using a transamination approach to access novel Fe(II) complexes, this study presents the synthesis, X-ray crystallographic and magnetic characterisation of a series of new iron complexes containing the multifunctional 2,2-dipyridylamide (DPA) ligand using iron bis(amide) [{Fe(HMDS)$_2$}$_2$] and sodium ferrate [{NaFe(HMDS)$_3$}$_\infty$] (**1**) as precursors (HMDS = 1,1,1,3,3,3-hexamethyldisilazide). Reactions of DPA(H) with **1** show exceptionally good stoichiometric control, allowing access to heteroleptic [(THF)$_2$·NaFe(DPA)(HMDS)$_2$] (**3**) and homoleptic [{THF·NaFe(DPA)$_3$}$_\infty$] (**4**) by using 1 and 3 equivalents of DPA(H) respectively. Linking this methodology and co-complexation, which is a more widely used approach to prepare heterobimetallic complexes, **3** can also be prepared by combining NaHMDS with heteroleptic [{Fe(DPA)(HMDS)}$_2$] (**2**). In turn, **2** has been also synthesised and structurally defined by reacting [{Fe(HMDS)$_2$}$_2$] with two equivalents of DPA(H). Structural studies demonstrate the coordination flexibility of the N-bridged bis(heterocycle) ligand DPA, with **2** and **3** exhibiting discrete monomeric motifs, whereas **4** displays a much more intricate supramolecular structure, with one of its DPA ligands coordinating in an *anti/anti* fashion (as opposed to **2** and **3** where DPA shows a *syn/syn* conformation), which facilitates propagation of the structure via its central amido N. Magnetic studies confirmed the high-spin electron configuration of the iron(II) centres in all three compounds and revealed the existence of weak ferromagnetic interactions in dinuclear compound **2** (J = 1.01 cm^{-1}).

Introduction

Advances in the development of cooperative heterobimetallic compounds and their application in synthesis continue to attract widespread interest.[1–4] Exhibiting unique synergistic properties, mixed-metal complexes (many of which can be categorised as ates) can effectively execute key organic transformations such as deprotonative metallation,[5] metal/halogen exchange[6] and nucleophilic addition;[7–9] outperforming in many cases traditional single-metal reagents.[10–13] To date, most of this research activity has concentrated on complexes which combine an alkali-metal with an s/p block lower polarity metal such as Mg, Zn or Al.[1–4,14,15] Examples of the remarkable reactivity of these systems include the regioselective alpha-metallation of THF and the *ortho-meta'* and *meta-meta'* di-magnesiations of a series of arenes with sodium magnesium template base [Na$_4$Mg$_2$(TMP)$_6$(^{n}Bu)$_2$] (TMP = 2,2,6,6-tetramethylpiperidide).[16] Efforts to match the successes observed with main-group systems with earth-abundant transition metals have so far been limited.[17–20] Iron's inherent abundance and benign nature presents many economical and ecological benefits,[21–24] but furthermore its open-shell character introduces a new dimension of interest not accessible to main-group systems, namely the potential to exhibit interesting magnetic behaviours.[25–31] Ferrate complexes[32–38] have garnered interest as potential key intermediates in Fe-catalysed C-C bond forming processes[39–42] and have shown the ability to mediate other important synthetic processes. Indeed, Mongin has reported metallation of aromatic and heteroaromatic substrates at ambient temperature using the putative lithium ferrate complex [LiFe(TMP)$_3$].[43] Closely related to this work, Knochel has demonstrated the synthesis of the Fe(II) complex [(TMP)$_2$Fe·4LiCl·2MgCl$_2$], capable of metallating functionalised arenes to undergo subsequent nickel-catalysed cross-couplings with alkyl halides.[44] Despite these insightful studies in organic synthesis, the structure or constitution of the proposed ferrate intermediates has not been forthcoming. In addition, Mulvey has reported structurally well-defined ferrate complex [Na$_4$Fe$_2$(TMP)$_6$(C$_6$H$_4$)], which promote the direct diferration of benzene.[45]

Other relevant structural studies include Layfield's work using Fe(HMDS)$_2$ (HMDS = 1,1,1,3,3,3-hexamethyldisilazide) to access of homo- and heterometallic Fe(II) cage complexes[46] as well as homoleptic tris(amido) lithium ferrate complexes.[47] In addition, we have also reported the ferration of N-heterocyclic carbene IPr (IPr = 1,3-bis(2,6-diisopropylphenyl)imidazol-2-ylidene) at its C4 position by sequential reactions with

[a] *WestCHEM, Department of Pure and Applied Chemistry, University of Strathclyde, 295 Cathedral Street, Glasgow, G1 1XL, U.K.*
[b] *Department de Química Inorgànica, Universitat de Barcelona, Diagonal 645, 08028 Barcelona, Spain*

† Electronic Supplementary Information (ESI) available: [Experimental Data, NMR spectra and magnetic studies]. See DOI: 10.1039/x0xx00000x

$NaCH_2SiMe_3$ and $Fe(HMDS)_2$.[48] Moreover, our studies on co-complexation reactions have shown that Na(HMDS) and $Fe(HMDS)_2$ undergo cocomplexation in non-donor solvents such as hexane to form novel polymeric solvent-free $[\{NaFe(HMDS)_3\}_\infty]$ (**1**) which exhibits an unusual polymeric chain structure.[48]

Building on these initial studies, here we explore the reactivity of this heterobimetallic complex in transamination reactions with 2,2'-dipyridylamine (DPA(H)) to access novel homo- and heteroleptic sodium ferrate complexes.

Although less prevalent throughout organometallic chemistry than HMDS,[49] amido DPA has been utilised in a number of varied branches of chemistry[50] including materials science,[51] catalysis,[52] supramolecular chemistry[53] and even in cooperative bimetallic chemistry.[54] Being the simplest of the poly 2,2'pyridyl amides, DPA can potentially coordinate through three N sites; one central amido N and two neutral pyridyl N atoms.[55] Rotation around the two N_{amido}-C bonds allows for DPA to adopt three different conformations; *syn/syn*, *syn/anti* and *anti/anti* (Fig. 1).[56] Within heterobimetallic chemistry, Mulvey has successfully prepared mixed sodium-zinc reagents containing this amide which can promote remote alkylation of benzophenone at the para position of one of its phenyl groups.[54]

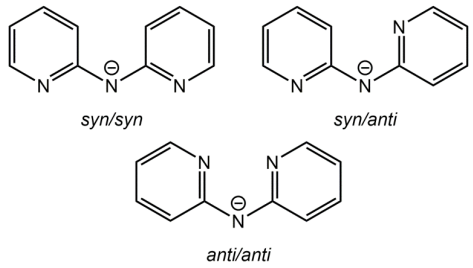

Fig. 1 Main conformational arrangements of 2,2'-dipyridylamide.

Results and Discussion

Synthetic and Structural Studies

We started our investigations with the uni-metal amide $Fe(HMDS)_2$, by reacting it with one molar equivalent of DPA(H) in hexane, which produced a brown solution with an off-white precipitate. Addition of THF afforded a homogeneous dark solution that upon cooling to −30°C deposited a crop of orange crystals of heteroleptic bis(amide) $[\{Fe(HMDS)(DPA)\}_2]$ (**2**) in an 88% yield (Scheme 1).

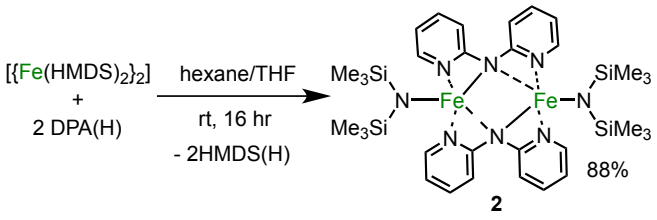

Scheme 1 Hemi-transamination of $Fe(HMDS)_2$ with DPA(H).

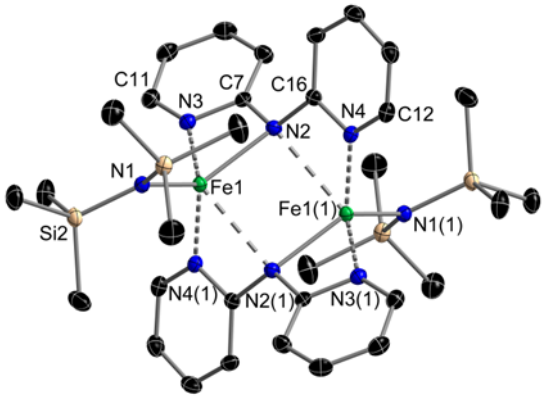

Fig. 2 Molecular structure of complex **2**. Hydrogen atoms omitted for clarity. Thermal ellipsoids displayed at 50% probability level. Selected bond distances (Å) and angles (°): Fe1-N1 1.9583(14), Fe1-N2 2.1642(14), Fe1-N3 2.2112(15), Fe1-N4(1) 2.1044(14), Fe1---N2(1) 2.546(1), Fe1---Fe1(1) 3.3609(1); N1-Fe1-N2 134.76(6), N1-Fe1-N3 119.34(6), N1-Fe1-N4(1) 111.04(6), N2-Fe1-N3 61.70(5), N2-Fe1-N4(1) 113.54(5), N3-Fe1-N4(1) 97.63(5), N1-Fe1---Fe1(1) 134.078(1).

As determined by X-ray crystallography, **2** displays a dimeric structure with a novel eight-membered {FeNCNFeNCN} core (Fig. 2). The symmetrically equivalent Fe centres are coordinated by HMDS in the terminal position whilst the DPA ligands assume bridging positions between the metal centres. The DPA ligands maximise coordination to the Fe centres through their neutral ring nitrogens with the pyridyl rings adopting a *syn/syn* conformation with an interplanar Py-N_{amido}-Py (Py = pyridyl) angle of 50.458°. Fe1 is formally five-coordinate when considering the long contact to the opposing central amido nitrogen (Fe1---N2(1) 2.546(1) Å); though much shorter bond distances are observed between Fe1 and amido nitrogens N1 and N2 (1.9583(14) and 2.1642(14) Å, respectively) and to pyridyl nitrogens N3 and N4(1) (2.2112(15) and 2.1044(14) Å, respectively). Discounting N2(1), a distorted tetrahedral geometry is present around Fe1 (average N-Fe-N angle = 106.36°, range 61.70(5)° to 134.76(6)°, excluding N2(1)). The Fe1---Fe1(1) separation in **2** is 3.3609(1) Å, considerably elongated from that of the equivalent Fe---Fe separation in $[\{Fe(HMDS)_2\}_2]$ at a distance of 2.663(2) Å.[57] Exhibiting good solubility in C_6D_6, the paramagnetic character of **2** was evidenced in the five broad paramagnetically shifted resonances observed in its ^{1}H NMR spectrum, ranging from 47.15 to −14.31 ppm and accounting for all hydrogen atoms of DPA along with a distinct broad singlet at 17.01 ppm integrating for 18H which can be assigned to the $SiMe_3$ groups. Attempts to measure the solution phase magnetic moment of **2** (via the Evans method at 300 K)[58,59] were inconclusive.

Whilst several Fe complexes containing the amine DPA(H) have been structurally defined,[60–62] there are only two examples where Fe is directly bonded to amide DPA.[63,64] The structure of **2** is reminiscent to that recently reported for $[\{Fe(Mes)(DPA)\}_2]$ resulting from the metallation of DPA(H) by bis(aryl) complex $[\{Fe(Mes)_2\}_2]$, where the DPA ligands also coordinate in a *syn-syn* fashion, bridging the Fe centres while

the mesityl groups are bound terminally.[63] Interestingly, despite the fact that 2 equivalents of DPA(H) are employed in the reaction, only one of mesityl groups can be replaced by the amide DPA, which contrasts with divergent reactivity observed with other first row transition metals (Cr, Co, Ni) which under the same conditions are able to form bis(amide) complexes $[M_2(DPA)_4]$.[63,65–69]

Encouraged by the successful hemi-transamination reaction using $Fe(HMDS)_2$, we next assessed the incorporation of DPA into sodium ferrate scaffolds, using a similar approach, by treating homoleptic **1** with appropriate amounts of the parent amine DPA(H) (Scheme 2).

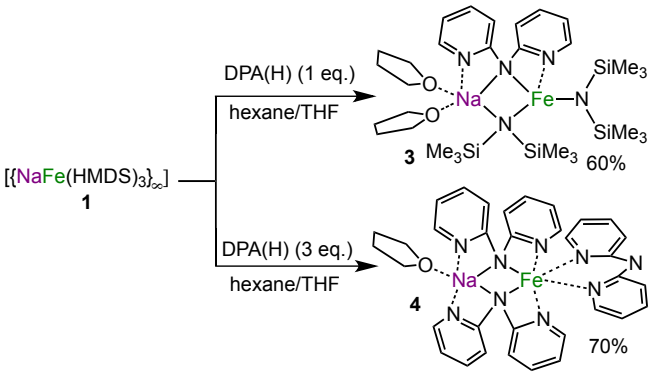

Scheme 2 Transamination of sodium ferrate **1** with 1 (top) and **3** (bottom) equivalents of DPA(H) .

Addition of one molar equivalent of DPA(H) to a solution of **1** in hexane immediately afforded a brown suspension which could be solubilised by introducing THF (Scheme 2, top). Orange crystals obtained at −30°C were found to be the sodium mixed-amido ferrate $[(THF)_2{\cdot}NaFe(DPA)(HMDS)_2]$ (**3**), recovered in a 60% yield. Interestingly, complex **3** was also found to be accessible by combining equimolar equivalents of mixed-amido iron complex **2** and NaHMDS in C_6D_6 (see Supporting Information).

X-ray crystallographic studies of **3** confirmed successful transamination with HMDS and the incorporation of one DPA ligand into the ferrate structure, which resides in a *syn/syn* conformation, acting as a bridge between Na1 and Fe1 to generate a monomeric dinuclear contacted ion-pair structure (Fig. 3). DPA's central amido nitrogen, N2, bridges between Fe1 and Na1 at distances of 2.1723(13) and 2.6710(15) Å, respectively, whilst neutral pyridyl nitrogens N1 and N3 provide additional coordination to Na1 and Fe1, respectively. The interplanar Py-N_{amido}-Py angle displayed by the DPA ligand in **3** is 44.281°, marginally more acute than in **2**.

As previously described for other mixed-metal systems, including sodium ferrate **1**,[48] *anchoring* and *ancillary* bonding modes are present in the molecular architecture of compound **3**.[70] The Fe(II) centre forms shorter and more covalent Fe-N_{amide} bonds [ranging from 1.9769(14) to 2.1723(13) Å], providing the foundation for the $\{Fe(DPA)(HMDS)_2\}^-$ anion to which the $\{Na(THF)_2\}^+$ cation is affixed by a combination of weaker Na-N ancillary bonds involving N2, N5 and N1. Notably a close inspection of the different metal-N(DPA) distances shows that while for iron both Fe-N_{amide} and Fe-$N_{pyridyl}$ are comparable [2.1723(13) and 2.1844(5) Å, respectively], in the case of Na, the interaction with the N of the pyridyl ring (N1 in Fig. 3) is stronger than that with N_{amide} (N2 in Fig. 3) [2.3822(17) and 2.6710(15) Å, respectively] which is consistent with significant delocalisation of the negative charge of the amido ligand within the pyridyl rings. As mentioned above, although alkali-metal amido ferrates have already shown interesting applications in synthesis, the number of structurally defined complexes is scarce. Related to **2**, Layfield has reported mixed lithium-iron (II) complex $[\{LiFe(BTA)(HMDS)_2\}_2]$ (BTA(H) = benzotriazole), which displays a dimeric structure with a central $\{Li(BTA)\}_2$ core capped on each end by a $Fe(HMDS)_2$ unit and has been prepared by a common salt-metathesis approach of Li(BTA) with $FeBr_2$.[46]

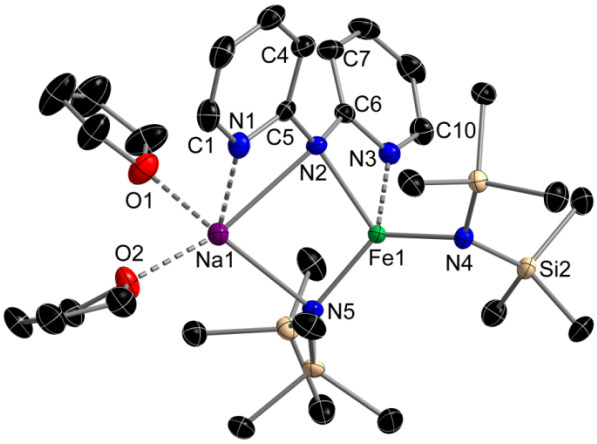

Fig. 3 Molecular structure of complex **3**. Hydrogen atoms and disorder present in the two THF molecules and one $SiMe_3$ unit omitted for clarity. Thermal ellipsoids displayed at 50% probability level. Selected bond distances (Å) and angles (°): Fe1-N2 2.1723(13), Fe1-N3 2.1844(14), Fe1-N4 1.9769(14), Fe1-N5 2.0171(14), Fe1---Na1 3.2253(7), Na1-N1 2.3822(17), Na1-N2 2.6710(15), Na1-N5 2.5464(15), Na1-O1 2.3479(15), Na1-O2 2.3425(14); N2-Fe1-N3 61.71(5), N2-Fe1-N4 118.24(6), N2-Fe1-N5 105.93(5), N3-Fe1-N4 103.30(6), N3-Fe1-N5 121.04(6), N4-Fe1-N5 128.42(6), Na1-N2-Fe1 82.82(5), Na1-N5-Fe1 89.16(5), Na1---Fe1-N4 145.19(4), N1-Na1-N2 53.62(5), N1-Na1-N5 119.96(5), N1-Na1-O1 91.84(6), N1-Na1-O2 98.80(6), N2-Na1-N5 79.73(5), N2-Na1-O1 94.22(5), N2-Na1-O2 152.28(5), N5-Na1-O1 131.07(6), N5-Na1-O2 118.20(5), O1-Na1-O2 88.84(5).

The ^1H NMR spectrum of **3** in C_6D_6 reveals one very broad resonance at 6.39 ppm and two marginally sharper resonances at 4.97 and 2.12 ppm. The extremely broad nature of the resonance at 6.39 ppm which also overlaps with the residual solvent signal and another resonance at 4.97 ppm, precludes a meaningful integration and assignment of the spectrum. The solution phase magnetic moment of **3** was found to be 4.93 μ_B (determined by Evans method at 300 K)[58,59] close to the expected value (4.90 μ_B) for a high-spin (S = 2) Fe(II) centre.

Introduction of 3 molar equivalents of DPA(H) to a hexane solution of **1** and stirring overnight generated a mustard coloured suspension in a brown solution (Scheme 2, bottom).

Recrystallisation from toluene/THF at −30°C furnished yellow plate-like crystals whose structure was established by X-ray crystallography to be polymeric [{THF·NaFe(DPA)$_3$}$_\infty$] (**4**) (Fig. 4), isolated in crystalline form in a 70% yield.

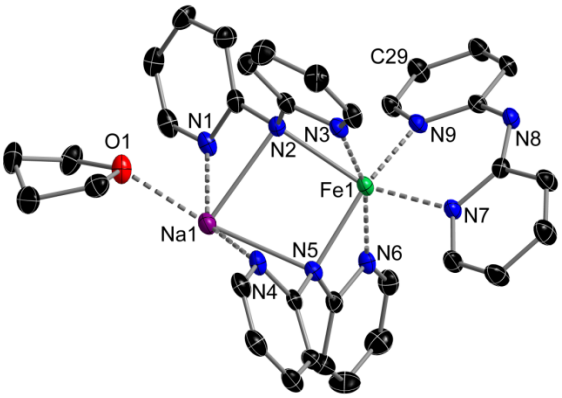

Fig. 4 Asymmetric unit of complex **4**. Hydrogen atoms and co-crystallised disordered toluene omitted for clarity. Thermal ellipsoids displayed at 30% probability level. Selected bond distances (Å) and angles (°): Fe1-N2 2.286(4), Fe1-N3 2.177(4), Fe1-N5 2.159(3), Fe1-N6 2.262(4), Fe1-N7 2.127(3), Fe1-N9 2.101(3), Fe1---Na1 3.4879(17), Na1-N1 2.512(4), Na1-N2 2.571(4), Na1-N4 2.602(4), Na1-N5 2.512(4), Na1-O1 2.362(4), Na1-N8(1) 2.480(4); N2-Fe1-N3 60.34(13), N2-Fe1-N5 92.97(13), N2-Fe1-N6 112.41(13), N2-Fe1-N7 152.05(14), N2-Fe1-N9 93.73(14), N3-Fe1-N5 103.05(14), N3-Fe1-N6 162.71(12), N3-Fe1-N7 92.74(14), N3-Fe1-N9 102.07(14), N5-Fe1-N6 60.46(13), N5-Fe1-N7 101.03(14), N5-Fe1-N9 154.03(14), N6-Fe1-N7 95.53(14), N6-Fe1-N9 93.87(13), N7-Fe1-N9 84.21(14), Na1-N2-Fe1 91.61(13), Na1-N5-Fe1 96.31(14), N1-Na1-N2 53.13(12), N1-Na1-N4 147.38(13), N1-Na1-N5 110.86(13), N1-Na1-O1 87.01(14), N1-Na1-N8(1) 103.22(13), N2-Na1-N4 94.31(12), N2-Na1-N5 78.73(12), N2-Na1-O1 94.62(13), N2-Na1-N8(1) 153.95(15), N4-Na1-N5 52.85(12), N4-Na1-O1 98.97(14), N4-Na1-N8(1) 108.15(14), N5-Na1-O1 149.71(14), N5-Na1-N8(1) 104.14(13), O1-Na1-N8(1) 94.72(13).

Complex **1** has undergone a complete three-fold transamination to release three equivalents of HMDS(H), incorporating three DPA ligands to furnish a new homoleptic sodium ferrate. Two DPA units bridge between Na1 and Fe1, residing in *syn/syn* conformations as seen in **3**. Contrastingly, the terminal DPA ligand adopts an *anti/anti* conformation, thus Fe1 is coordinated by the two pyridyl nitrogens N7 and N9 (2.127(3) and 2.101(3) Å, respectively), whilst bridgehead amido N8 points away to a sodium atom of a second monomer unit [at a distance of 2.480(4) Å] to give a novel 1D polymeric chain (Fig. 5).

The hexacoordinated Fe(II) centre resides in a highly distorted N_6-octahedral environment [NFeN angles ranging from 60.34(13)° to 162.71(12)°]. Along with the pseudo-terminal DPA ligand with an *anti/anti* conformation (vide supra), Fe1 completes its coordination by bonding to amido N2 and N5 at distances of 2.286(4) and 2.159(3) Å, respectively and two further pyridyl N3 and N6 at distances of 2.177(4) and 2.262(4) Å, respectively. The sodium atom engages the two bridging DPA ligands through their amido N and one of their pyridyl rings (N2, N5 and N1, N4 respectively) giving rise to interactions of similar strength despite the different types of N atoms involved in the bonding [Na-N distances ranging from 2.512(4) to 2.602(4) Å]. Coordinative saturation is achieved by THF ligation and by interacting with the amido N of a DPA ligand from a neighbouring unit (N8), which allows the propagation of the polymeric structure (vide supra, Fig. 5). Noticeably this supramolecular Na-N interaction [2.480(4) Å] is shorter than those observed within the asymmetric unit of **4** (average Na-N 2.549 Å).

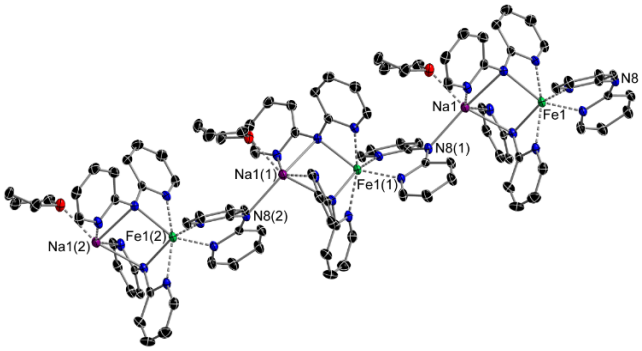

Fig. 5 Section of polymeric chain of **4** showing propagation and selected atom labelling, Na1-N8(1) 2.480(4) Å. Hydrogen atoms and co-crystallised disordered toluene omitted for clarity. Thermal ellipsoids displayed at 30% probability level.

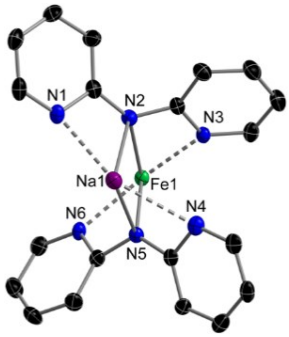

Fig. 6 Alternative view of the Na/Fe core and two bridging DPA ligands of **4**. Hydrogen atoms omitted for clarity. Thermal ellipsoids displayed at 30% probability level.

In addition, the bridging DPA ligands in **4** effectively mirror one another by significant twisting of the pyridyl rings from the {Na1-N2-Fe1-N5} core plane, maximising $N_{pyridyl}$ coordination to both metal centres (Fig. 6). Incorporating two bridging DPA groups in *syn/syn* conformations, translates in an appreciably larger Na---Fe separation [3.4879(17) Å] in **4** when compared to sodium ferrates **1** [3.0131(13) Å] and **3** [3.2253(7) Å]. Whilst the interplanar Py-N_{amido}-Py angle of 50.465° for N2 DPA ligand has a similar value to the corresponding angles observed in complexes **2** and **3**, the N5 bridging DPA ligand displays a far more acute interplanar angle of 39.444°, whilst an acuter still angle of 24.384° is observed for the N8 terminal DPA ligand in **4**.

Similarly to **3**, the ^{1}H NMR spectrum of **4** in C_6D_6 displayed a number of poorly resolved, broad and overlapping signals

(between 0 and 30 ppm) which precluded a meaningful assignment of resonances. The solution-phase magnetic moment of **4** (5.30 μ_B) was determined using the Evans method[58,59] (at 300 K) and is consistent with a high-spin Fe(II) $S = 2$ configuration.

As far as we can ascertain, complexes **3** and **4** constitute the first examples in ferrate chemistry, to incorporate DPA in their constitution, which have been prepared and structurally defined. Looking beyond iron but staying within mixed-metal chemistry, Mulvey's sodium zincates $[(TMEDA)_2Na_2(\mu\text{-}DPA)_2Zn(^tBu)_2]$ and $[Na(THF)_6]^+[Zn(^tBu)_2(DPA)Zn(^tBu)_2]^-$ are worthy of comment.[54] In the former structure, one DPA bridges *syn/syn* between two Na atoms and another bridges in *anti/anti* conformation with N_{amido} centred between the Na atoms and the pyridyl N atoms coordinating to Zn. In contrast, the latter solvent-separated ion pair, has a single unit of DPA sandwiched between two Zn centres in an *anti/anti* conformation. From a more general perspective, Coronado has described the design of several mixed-metal chains containing oxalate ligands, including trimetallic complex $[K(18\text{-crown-6})]^+[Co(DPA)Fe(ox)_3]^-$ (ox = oxalate),[71] which exhibits interesting magnetic properties although the DPA ligand in this system coordinates exclusively to Co.

Magnetic Studies

The electronic structure of Fe(II) in complexes **2**, **3** and **4** was studied through bulk magnetisation measurements and for **2**, EPR spectroscopy. Thus, molar paramagnetic susceptibility (χ_M) data were collected on microcrystalline samples from 2 to 300 K, under a constant magnetic field of 0.5 T. Additionally, field dependent (0 to 5 T) magnetisation measurements at 2 K were performed.

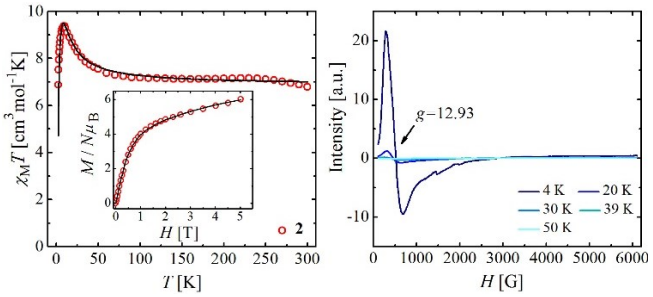

Fig. 7 *Left*: $\chi_M T$ *vs* T and $M/N\mu_B$ *vs* H (inset) curves of compound **2** with the best fit (solid line, see text for details). *Right*: Variable temperature X-band EPR spectra of a powdered sample of complex **2**.

The $\chi_M T$ *vs* T plot for **2** (Fig. 7) at 300 K features a value of $\chi_M T$ of 6.79 cm^3 K mol^{-1}, which is higher than expected for two non-interacting high-spin (HS; $S = 2$) Fe(II) centres (6.00 cm^3 K mol^{-1} if $g = 2.0$). The anomalous tail in this temperature region is attributed to marginal decomposition of the sample upon warming. A g factor of 2.13, revealing the coupling of an unquenched angular momentum to the electronic spin is estimated using the Curie Law near ambient temperature. This point is reached from a maximum of 9.37 cm^3 K mol^{-1} at 9 K, which is followed by a sharp decrease that becomes smoother after 50 K. The maximum is attained through a sharp increase from a $\chi_M T$ value of 6.88 cm^3 K mol^{-1} at 2 K. The latter pattern is ascribed to the effects of the zero-field splitting (ZFS). These effects are corroborated by the $M/N\mu_B$ *vs* H curve, which does not reach saturation at the highest magnetic field (it reaches 6.02 μ_B at 5 T, while the expected value is 8 μ_B for $g = 2.0$ and $S = 4$ or two $S = 2$).

A simultaneous fit of both curves was carried out using the program PHI[72] by matrix diagonalisation of the (perturbative) anisotropic spin Hamiltonian defined in Equation 1:

$$\hat{H} = D\sum_i \left(\hat{S}_{iz}{}^2 - \frac{1}{3}\hat{S}_i{}^2\right) + E\sum_i \left(\hat{S}_{ix}{}^2 - \hat{S}_{iy}{}^2\right) + g\mu_B B\sum_i \hat{S}_i - 2J\left(\hat{S}_1\hat{S}_2\right) \quad (1)$$

In Eq. 1, J is the exchange constant, $\hat{S}_{ij}$ ($i = 1, 2$; $j = x, y, z$) is the total spin operator of the individual Fe(II) ions, B is the magnetic induction and μ_B is the Bohr magneton, while D and E stand for axial and rhombic ZFS parameters, respectively. To avoid the overparameterisation of the Hamiltonian, the isotropic g factor was fixed at 2.14. The best fit produced J = 1.01 cm^{-1}, D = 7.31 cm^{-1} and $|E|$ = 1.36 cm^{-1}, together with a small intermolecular interaction zJ = 0.02 cm^{-1}. Considering that negative values of D have been reported for other trigonal-pyramidal Fe(II) complexes,[73,74] a second set of parameters with negative D was explored, yielding J = 0.93 cm^{-1}, D = –5.59 cm^{-1} and $|E|$ = 1.45 cm^{-1}. The latter presents slightly higher deviations from the experiment at low temperature. In both cases, large values of the rhombic ZFS parameter E reflect significant distortions of the basal FeN_3 plane from the ideal three-fold symmetry. However, a positive sign of D can be anticipated by the strong distortion of the coordination geometry of **2** with respect to the highly regular trigonal-pyramidal symmetry reported by Long *et al*.[73,74] Instead, the ligand field in **2** brings it closer to a very distorted tetrahedral geometry, which in d^6 ions is expected to cause positive D values.[75]

The magnetic exchange between both Fe centres in the complex is consistent with the short distance (3.3611(6) Å) mediating between them. The most likely mechanism of this exchange is the spin polarisation of ligand centred electronic clouds spread over each of the N–C–N moieties of DPA bridging the metals and orthogonal to some of the magnetic orbitals of the latter. The unusual coordinating mode seen in **2** was also reported for the compound $[\{Fe(Mes)(DPA)\}_2]$.[63] In the absence of magnetic studies, DFT calculations confirmed the HS state of the Fe(II) ions and local spin densities of 3.62 at these centres (thus showing the S = 4 ground state). Ferromagnetic coupling within Fe(II) dinuclear complexes incorporating similar bridging motifs was also reported for $[Fe_2L_4](ClO_4)_4$ (L= 1,13,14-triaza-dibenz[*a,j*]anthracene)[76] and $[Fe_2Br_3(trop_2AM)]$ (H-trop$_2$AM = *N,N'*-bis-trop-phenylamidine).[77]

Variable temperature EPR (Fig. 7) mirrors the magnetic behaviour of **2** described above, thus confirming the Fe oxidation state of +2. The latter is obvious from the fact that

the sample is EPR silent above 40 K. Down to 20 K, one resonance becomes apparent in the low-field region (*g* value of 12.93) increasing in intensity upon cooling. The observed spectral feature is related to the *S* = 4 state of the Fe(II) dimer where a forbidden transition occurs between the *M*s levels +4 and –4 (Δ*M*s = 8) which are split in zero magnetic field by ~E^2/D.[78]

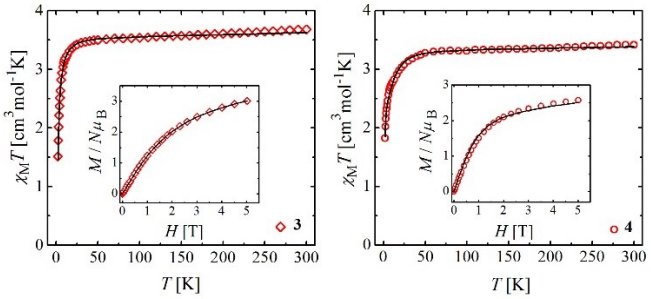

Fig. 8 *$\chi_M T$ vs T and $M/N\mu_B$ vs H (inset) curves of compounds **3** and **4** with their best fit (solid line, see text for details)..*

For compounds **3** and **4**, the $\chi_M T$ value at 300 K is (in the **3**/**4** format) 3.682/3.417 cm³ K mol⁻¹ (Fig. 8), higher than expected for an isolated HS (*S* = 2) Fe(II) centre (calculated as 3.00 cm³ K mol⁻¹ for *g* = 2.0) because of the effect of unquenched angular momentum. This yields a Curie Law estimated *g* factor of 2.22/2.13. The $\chi_M T$ vs *T* plot shows a nearly constant value with only a slightly positive slope as a result of temperature independent paramagnetism (TIP) estimated as 330/250 x 10⁻⁶ cm³ mol⁻¹. Below 40 K, the curve drops abruptly down to 1.52/1.83 cm³ K mol⁻¹ at 2 K. The cause of this decline is the ZFS of the metal ions, which is also evident from the isothermal (2 K) $M/N\mu_B$ *vs H* curves (Fig. 8), since the values from the latter at the highest magnetic fields are far from saturation (with a measured value of 3.01/2.57 μ_B compared to the expected of 4 μ_B for *g* = 2 and *S* = 2). Simultaneous fitting of both sets of data using the spin Hamiltonian defined in Eq. 2, yielded the parameters *D* = 6.70/–10.48 cm⁻¹ and |*E*| = 0.67/0.79 cm⁻¹ as well as weak intermolecular interaction constants *zJ* = 0.02/0.01 cm⁻¹. In these fits, an isotropic *g* factor and a TIP value were fixed at 2.17/2.10 and 330/250 x10⁻⁶ cm³ mol⁻¹, respectively.

$$\hat{H} = D\left(\hat{S}_z{}^2 - \frac{1}{3}\hat{S}^2\right) + E\left(\hat{S}_x{}^2 - \hat{S}_y{}^2\right) + \mu_B \hat{S} g B \qquad (2)$$

For both compounds, attempts to simulate the data employing opposite signs for *D* were unsuccessful. The positive *D* value of **3** is consistent with that obtained for **2** given the large similarity of their coordination geometries.

Although the N_6 coordination environment around the metal centre in **4** could be appropriate for the appearance of thermally induced spin-crossover, the experimental results show that this ion centre stays trapped in the HS state, as indicated by the crystal structure (Fe–N bond lengths at 123 K >2.1Å). The likely explanation is that the large distortions from the ideal octahedral geometry imposed by the ligands cause the putative LS state to possess higher enthalpy than the HS state.[79] The evaluation of the local distortion from the ideal octahedron at the Fe(II) ion in **4** using the parameters *Σ* and *Θ* gave 142.4(5)° and 503.7(10)°, respectively, which fall into the reported ranges typical for the HS state.[80–83] These findings are also consistent with reported magnetic data for other compounds with identical coordination geometry.[84,85]

The possibility that compounds **2** to **4** exhibit slow relaxation of the magnetisation was evaluated by means of dynamic magnetisation measurements. Thus, experiments under an oscillating (AC) field of 4 Oe were performed under zero or 1000 Oe applied constant field (Figs. S5 to S7). These measurements yielded, for all three compounds, superimposed curves for the in-phase magnetic susceptibility (χ_M') and no signal for the out-of-phase component (χ_M''). The lack of single molecule magnet (SMM) behaviour for **4** (which could be anticipated, given its large and axial ZFS parameter; *D* = –10.48 cm⁻¹) can be rationalised with the existence of significant rhombic anisotropy, which likely accelerates the quantum tunnelling of magnetisation, as is known for the non-Kramers ions such as high-spin Fe(II).

Conclusions

On studying transamination reactions of sodium ferrate [{NaFe(HMDS)$_3$}$_\infty$] (**1**) and its parent iron bis(amide) Fe(HMDS)$_2$ with 2,2'-dipyridylamine DPA(H), three new iron complexes have been isolated and structurally defined containing the N-bridged bis(heterocyclic) ligand DPA. In stoichiometrically controlled processes, reacting **1** with 1 or 3 equivalents of DPA(H) generates the sodium ferrates [(THF)$_2$·NaFe(DPA)(HMDS)$_2$] (**3**) and [{THF·NaFe(DPA)$_3$}$_\infty$] (**4**) respectively. Interestingly **3** can also be prepared using an alternative co-complexation approach by combining heteroleptic [{Fe(HMDS)(DPA)}$_2$] (**2**) with the sodium amide NaHMDS. Highlighting the coordination flexibility of this multifunctional amido ligand, structural studies revealed that while in **2** and **3** DPA adopts a *syn/syn* conformation, acting as a bridge between two metal centres, in homoleptic complex **4**, two DPA ligands present the same type of conformation, whereas a remaining DPA group binds in an *anti/anti* fashion, facilitating formation of a novel intricate polymeric chain structure. SQUID magnetisation measurements confirmed the structural findings by establishing the presence of ferromagnetically coupled (compound **2**, *J* = 1.01 cm^{-1}) and isolated high-spin Fe(II) centres (*S* = 2) in compounds **3** and **4**. Evaluation of the ZFS parameters yielded positive *D* values for the spin carriers in **2** and **3**, with similar five-coordination geometries, and negative for compound **4**, consistent with its the octahedral geometry. Despite its negative *D* = –10.48 cm⁻¹ parameter, this compound does not show slow relaxation of magnetisation.

Collectively these findings advance the synthesis of alkali-metal ferrates and the understanding of the intriguing structural/reactivity/magnetic correlations in this class of mixed-metal reagents. While alkali-metal ferrates have already shown significant promise in synthesis, the number of

methods available to access these systems remains scarce. These findings reveal the potential that transamination approaches offer, using tris(amido) sodium ferrate **1** as a precursor, to gain entry to other homo- and heteroleptic heterobimetallic complexes.

Experimental

General Conditions

All reactions were carried out under an inert dry argon atmosphere utilising standard Schlenk and glove-box techniques (MBraun, MB10 Compact, <0.5 ppm H_2O, O_2). NaHMDS and 2,2'-dipyridylamine were purchased from Sigma Aldrich and used as received. $Fe(HMDS)_2$ was prepared according to a modified literature procedure from Lappert *et al*.[48,86] Hexane was dried prior to synthesis by Grubbs column (PureSolv micro solvent purification system, Innovative Technologies) to remove any traces of moisture and dissolved oxygen and stored over 4 Å molecular sieves. Toluene and THF were used immediately after being freshly distilled over sodium benzophenone ketyl under nitrogen. Deuterated solvent C_6D_6 for NMR spectroscopy was stored over 4 Å molecular sieves in the glove-box prior to use. NMR spectroscopy samples for complexes **2**, **3** and **4** were prepared inside the inert argon atmosphere of the glove-box. ^1H (400.13 MHz) NMR spectra were recorded on either a Bruker AV400 or AV3 spectrometer using TopSpin (v2.1, Bruker Biospin, Karlsruhe) at 300 K. ^1H NMR spectra were referenced internally to the corresponding residual protio solvent peaks. Solution magnetic susceptibilities were determined by the Evans method at 300 K.[58,59] Elemental analyses were performed on a Perkin Elmer 2400 Series II CHNS/O Analyser. Single-crystal X-ray diffraction was performed on Oxford Diffraction Xcalibur and Gemini diffractometers at 123 K using Mo Kα (λ = 0.71073 Å) or Cu Kα radiation (λ = 1.54178 Å), respectively. The structures were solved by direct methods and refined on all unique F2 values using the SHELXS[87] and SHELXL[88] package within either the WinGX[89] or ShelXle[90] GUIs

Synthetic Procedures

[{NaFe(HMDS)$_3$}$_\infty$] (1) Hexane solutions of complex **1** were prepared *in situ* according to the previously reported method.[48]

[{Fe(HMDS)(DPA)}$_2$] (2) $Fe(HMDS)_2$ (0.754 g, 2 mmol) and DPA(H) (0.342 g, 2 mmol) were added to a Schlenk tube along with 20 mL of hexane. Upon stirring a brown solution with off-white precipitate was formed which was stirred at ambient temperature overnight. Addition of 8 mL of THF dissolved the precipitate and gave a black solution which was cooled to −30°C. This yielded orange plate-like crystals which were separated from solution and washed once with 3 mL of cold hexane (0.68 g, 88% yield). ^1H NMR (C_6D_6, 300 K) δ (ppm) = 47.15 [bs, DPA aryl C*H*'s, 2H], 25.00 [bs, DPA aryl C*H*'s, 2H], 21.27 [bs, DPA aryl C*H*'s, 2H], 17.01 [vbs, Si*Me*$_3$, 54H], −14.31 [bs, DPA aryl C*H*'s, 2H]. Anal. Calcd for $C_{32}H_{52}Fe_2N_8Si_4$: C 49.73, H 6.78, N 14.50 Found: C 49.94, H 6.78, N 14.80

[(THF)$_2$·NaFe(DPA)(HMDS)$_2$] (3) To a 1 mmol hexane solution of **1**, 0.171 g of DPA(H) (1 mmol) was added via solid addition tube resulting in the immediate formation of sticky tan/brown solid residue at the base of the Schlenk tube in the green solution. After stirring overnight at ambient temperature this residue was a dark brown suspension in the green solution, addition of 2 mL of THF gave a black solution. Cooling to −30°C allowed for the isolation of orange plate-like crystals (0.43 g, 60%). Complex **3** was also accessed via the addition of 0.0073 g (0.04 mmol) NaHMDS to a C_6D_6 solution of 2 (0.0155 g, 0.04 mmol) in a Young's NMR tube and refluxing for 90 minutes. Anal. Calcd for $C_{26}H_{52}FeN_5NaOSi_4$ (note that a molecule of THF is loss under vacuum): C 41.67, H 10.17, N 6.63 Found: C 41.24, H 9.99, N 7.16. Solution Magnetic Moment (C_6D_6, 300 K) = 4.93 μ_B

[{THF·NaFe(DPA)$_3$}$_\infty$] (4). To a 1 mmol solution of 1 in hexane, 0.513 g of DPA(H) (3 mmol) was added via solid addition tube resulting in the immediate formation of sticky tan/brown solid residue at the base of the Schlenk tube in the green solution. After stirring overnight at ambient temperature there was a mustard coloured suspension in a dark brown solution. All volatiles were removed under vacuum and the mustard coloured solid residue was redissolved in 15 mL of toluene and 5 mL of THF. Cooling to −30°C allowed for the isolation of yellow plate-like crystals (0.49 g, 70% yield). ^1H NMR (C_6D_6, 300 K) δ (ppm) = meaningful integration and assignment of proton resonances not possible. Anal. Calcd for $C_{75}H_{72}Fe_2N_{18}Na_2O_2$ (2 monomer units + 1 eq. of co-crystallised toluene): C 63.65, H 5.13, N 17.82 Found: C 63.54, H 5.13, N 18.14. Solution Magnetic Moment (C_6D_6, 300 K) = 5.30 μ_B.

Acknowledgements

We thank the EPSRC and the European Research Council (ERC) for their generous sponsorship of this research. We also thank Professor Robert E. Mulvey for his insightful comments.

Notes and references

1 R. E. Mulvey, F. Mongin, M. Uchiyama and Y. Kondo, *Angew. Chem. Int. Ed.*, 2007, **46**, 3802–24.
2 R. E. Mulvey and S. D. Robertson, *Top. Organomet. Chem.*, 2013, **47**, 129–158.
3 A. Harrison-Marchand and F. Mongin, *Chem. Rev.*, 2013, **113**, 7470–562.
4 F. Mongin and A. Harrison-Marchand, *Chem. Rev.*, 2013, **113**, 7563–727.
5 R. E. Mulvey, *Acc. Chem. Res.*, 2009, **42**, 743–55.
6 D. Tilly, F. Chevallier, F. Mongin and P. C. Gros, *Chem. Rev.*, 2014, **114**, 1207–1257.
7 E. Hevia, G. W. Honeyman, A. R. Kennedy and R. E. Mulvey, *J. Am. Chem. Soc.*, 2005, **127**, 13106–7.
8 S. E. Baillie, V. L. Blair, D. C. Blakemore, D. Hay, A. R. Kennedy, D. C. Pryde and E. Hevia, *Chem. Commun.*, 2012, **48**, 1985–7.
9 E. Crosbie, A. R. Kennedy, R. E. Mulvey and S. D. Robertson, *Dalt. Trans.*, 2012, **41**, 1832.

10 A. Krasovskiy and P. Knochel, *Angew. Chem. Int. Ed.*, 2004, **43**, 3333–6.
11 E. Hevia and R. E. Mulvey, *Angew. Chem. Int. Ed.*, 2011, **50**, 6448–50.
12 R. E. Mulvey, *Dalt. Trans.*, 2013, **42**, 6676–93.
13 L. Lochmann, *Eur. J. Inorg. Chem.*, 2000, 1115–1126.
14 R. E. Mulvey, *Organometallics*, 2006, **25**, 1060–1075.
15 M. Uchiyama and C. Wang, *Top. Organomet. Chem.*, 2014, **47**, 159–202.
16 A. J. Martínez-Martínez, A. R. Kennedy, R. E. Mulvey and C. T. O'Hara, *Science*, 2014, **346**, 834–837.
17 M. Uzelac, I. Borilovic, M. Amores, T. Cadenbach, A. R. Kennedy, G. Aromí and E. Hevia, *Chem. - A Eur. J.*, 2016, **22**, 4843–4854.
18 J. Garcia-Álvarez, A. R. Kennedy, J. Klett and R. E. Mulvey, *Angew. Chem. Int. Ed.*, 2007, **119**, 1123–1126.
19 L. M. Carrella, W. Clegg, D. V. Graham, L. M. Hogg, A. R. Kennedy, J. Klett, R. E. Mulvey, E. Rentschler and L. Russo, *Angew. Chem. Int. Ed.*, 2007, **46**, 4662–4666.
20 C. G. Werncke, E. Suturina, P. C. Bunting, L. Vendier, J. R. Long, M. Atanasov, F. Neese and S. Sabo-etienne, *Chem. - A Eur. J.*, 2015, 1–8.
21 C. Bolm, J. Legros, J. Le Paih and L. Zani, *Chem. Rev.*, 2004, **104**, 6217–54.
22 W. M. Czaplik, M. Mayer, J. Cvengros and A. J. von Wangelin, *ChemSusChem*, 2009, **2**, 396–417.
23 E. Nakamura and N. Yoshikai, *J. Org. Chem.*, 2010, **75**, 6061–7.
24 B. Su, Z. C. Cao and Z. J. Shi, *Acc. Chem. Res.*, 2015, **48**, 886–896.
25 R. A. Layfield, *Organometallics*, 2014, **33**, 1084–1099.
26 J. M. Frost, K. L. M. Harriman and M. Murugesu, *Chem. Sci.*, 2016, **7**, 2470–2491.
27 E. Bill, *Nat. Chem.*, 2013, **5**, 556–557.
28 P.-H. Lin, N. C. Smythe, S. I. Gorelsky, S. Maguire, N. J. Henson, I. Korobkov, B. L. Scott, J. C. Gordon, R. T. Baker and M. Murugesu, *J. Am. Chem. Soc.*, 2011, **133**, 15806–9.
29 C. G. Werncke, P. C. Bunting, C. Duhayon, J. R. Long, S. Bontemps and S. Sabo-Etienne, *Angew. Chem. Int. Ed.*, 2015, **54**, 245–248.
30 M. Atanasov, J. M. Zadrozny, J. R. Long and F. Neese, *Chem. Sci.*, 2013, **4**, 139–156.
31 J. M. Zadrozny, D. J. Xiao, M. Atanasov, G. J. Long, F. Grandjean, F. Neese and J. R. Long, *Nat. Chem.*, 2013, **5**, 577–581.
32 L. E. Aleandri, B. Bogdanovic, C. Diirr, A. Gaidies, T. Hartwig, S. C. Huckett, M. Lagarden, U. Wilczok and R. a Brand, *Chem. Mater.*, 1995, **7**, 1153–1170.
33 T. Kauffmann, *Angew. Chem. Int. Ed.*, 1996, **35**, 386–403.
34 A. Fürstner, H. Krause and C. W. Lehmann, *Angew. Chem. Int. Ed.*, 2006, **45**, 440–444.
35 A. Fürstner, R. Martin, H. Krause, G. Seidel, R. Goddard and C. W. Lehmann, *J. Am. Chem. Soc.*, 2008, **130**, 8773–87.
36 O. García Mancheño, *Angew. Chem. Int. Ed.*, 2011, **50**, 2216–8.
37 R. B. Bedford, P. B. Brenner, E. Carter, P. M. Cogswell, M. F. Haddow, J. N. Harvey, D. M. Murphy, J. Nunn and C. H. Woodall, *Angew. Chem. Int. Ed.*, 2014, **53**, 1804–1808.
38 M. H. Al-Afyouni, K. L. Fillman, W. W. Brennessel and M. L. Neidig, *J. Am. Chem. Soc.*, 2014, **136**, 15457–15460.
39 A. Fürstner, A. Leitner, M. Méndez and H. Krause, *J. Am. Chem. Soc.*, 2002, **124**, 13856–13863.
40 R. Martin and A. Fürstner, *Angew. Chem. Int. Ed.*, 2004, **43**, 3955–3957.
41 B. D. Sherry and A. Fürstner, *Acc. Chem. Res.*, 2008, **41**, 1500–11.
42 A. Fürstner, *Angew. Chem. Int. Ed.*, 2014, **53**, 8587–8598.
43 E. Nagaradja, F. Chevallier, T. Roisnel, V. Jouikov and F. Mongin, *Tetrahedron*, 2012, **68**, 3063–3073.
44 S. H. Wunderlich and P. Knochel, *Angew. Chem. Int. Ed.*, 2009, **48**, 9717–20.
45 P. Alborés, L. M. Carrella, W. Clegg, P. García-Alvarez, A. R. Kennedy, J. Klett, R. E. Mulvey, E. Rentschler and L. Russo, *Angew. Chem. Int. Ed.*, 2009, **48**, 3317–21.
46 S. A. Sulway, D. Collison, J. J. W. McDouall, F. Tuna and R. A. Layfield, *Inorg. Chem.*, 2011, **50**, 2521–6.
47 S. N. König, D. Schneider, C. Maichle-Mössmer, B. M. Day, R. A. Layfield and R. Anwander, *Eur. J. Inorg. Chem.*, 2014, **2014**, 4302–4309.
48 L. C. H. Maddock, T. Cadenbach, A. R. Kennedy, I. Borilovic, G. Aromí and E. Hevia, *Inorg. Chem.*, 2015, **54**, 9201–9210.
49 R. E. Mulvey and S. D. Robertson, *Angew. Chem. Int. Ed.*, 2013, **52**, 11470–87.
50 D. W. Brogden and J. F. Berry, *Comments Inorg. Chem.*, 2016, **36**, 17–37.
51 J. J. Kim and J. Yoon, *Inorg. Chim. Acta*, 2013, **394**, 506–511.
52 N. Madern, B. Talbi and M. Salmain, *Appl. Organomet. Chem.*, 2013, **27**, 6–12.
53 M. Burgos, O. Crespo, M. C. Gimeno, P. G. Jones and A. Laguna, *Eur. J. Inorg. Chem.*, 2003, 2170–2174.
54 D. R. Armstrong, J. A. Garden, A. R. Kennedy, R. E. Mulvey and S. D. Robertson, *Angew. Chem. Int. Ed.*, 2013, **52**, 7190–7193.
55 H. Schödel, C. Näther, H. Bock and F. Butenschön, *Acta Crystallogr. Sect. B Struct. Sci.*, 1996, **52**, 842–853.
56 F. A. Cotton, L. M. Daniels, G. T. Jordan IV and C. A. Murillo, *Polyhedron*, 1998, **17**, 589–597.
57 M. M. Olmstead, P. P. Power and S. C. Shoner, *Inorg. Chem.*, 1991, **30**, 2547–2551.
58 D. F. Evans, *J. Chem. Soc.*, 1959, 2003.
59 E. M. Schubert, *J. Chem. Educ.*, 1992, **69**, 62.
60 J. Y. Lu, T. J. Schroeder, A. M. Babb and M. Olmstead, *Polyhedron*, 2001, **20**, 2445–2449.
61 A. B. Gaspar, G. Agustí, V. Martínez, M. C. Codes, Muñoz, G. Levchenko and J. A. Real, *Inorg. Chim. Acta*, 2005, **358**, 4089–4094.
62 R. Carballo, B. Covelo, E. M. Vázquez-López, E. García-Martínez, A. Castiñeiras and C. Janiak, *Zeitschrift fur Anorg. und Allg. Chemie*, 2005, **631**, 2006–2010.
63 J. Sundberg, M. S. Vad, J. E. McGrady, P. M. Björemark, M. Håkansson and C. J. McKenzie, *J. Organomet. Chem.*, 2015, **786**, 40–47.
64 F. A. Cotton, L. M. Daniels, G. T. Jordan IV, C. A. Murillo and I. Pascual, *Inorg. Chim. Acta*, 2000, **297**, 6–10.
65 J. J. H. Edema, S. Gambarotta, A. Meetsma, A. L. Spek, W. J. J. Smeets and M. Y. Chiang, *J. Chem. Soc. Dalt. Trans.*, 1993, 789.
66 F. A. Cotton, L. M. Daniels, C. a Murillo and I. Pascual, *Inorg. Chem. Commun.*, 1998, **1**, 1–3.
67 M.-C. Suen, Y.-Y. Wu, J.-D. Chen, T.-C. Keng and J.-C. Wang, *Inorg. Chim. Acta*, 1999, **288**, 82–89.
68 J. F. Berry, F. A. Cotton, C. Lin and C. A. Murillo, *J. Clust. Sci.*, 2004, **15**, 531–541.
69 M. Nippe, G. H. Timmer and J. F. Berry, *Chem. Commun.*, 2009, 4357–9.
70 R. E. Mulvey, *Chem. Commun.*, 2001, 1049–1056.
71 E. Coronado, J. R. Galán-Mascarós and C. Martí-Gastaldo, *CrystEngComm*, 2009, **11**, 2143.
72 N. F. Chilton, R. P. Anderson, L. D. Turner, A. Soncini and K. S. Murray, *J. Comput. Chem.*, 2013, **34**, 1164–1175.
73 D. E. Freedman, W. H. Harman, T. D. Harris, G. J. Long, C. J. Chang and J. R. Long, *J. Am. Chem. Soc.*, 2010, **132**, 1224–5.
74 W. H. Harman, T. D. Harris, D. E. Freedman, H. Fong, A. Chang, J. D. Rinehart, A. Ozarowski, M. T. Sougrati, F.

Grandjean, G. J. Long, J. R. Long and C. J. Chang, *J. Am. Chem. Soc.*, 2010, **132**, 18115–18126.
75 S. Gomez-Coca, E. Cremades, N. Aliaga-Alcalde and E. Ruiz, *J. Am. Chem. Soc.*, 2013, **135**, 7010–7018.
76 W.-Z. Wang, C.-L. Hsieh, R. H. Ismayilov, C.-H. Hsu, I. P.-C. Liu, Y.-H. Liu, G.-H. Lee and S.-M. Peng, *New J. Chem.*, 2012, **36**, 2340–2346.
77 C. Lichtenberg, M. Adelhardt, M. Wörle, T. Büttner, K. Meyer and H. Grützmacher, *Organometallics*, 2015, **34**, 3079–3089.
78 M. P. Hendrich, E. P. Day, C.-P. Wang, B. S. Synder, R. H. Holm and E. Munck, *Inorg. Chem.*, 1994, **33**, 2848–2856.
79 J. M. Holland, J. A. McAllister, C. A. Kilner, M. Thornton-Pett, A. J. Bridgeman and M. A. Halcrow, *J. Chem. Soc. Dalt. Trans.*, 2002, **2**, 548–554.
80 J. K. McCusker, A. L. Rheingold and D. N. Hendrickson, *Inorg. Chem.*, 1996, **35**, 2100–2112.
81 M. Marchivie, P. Guionneau, J.-F. Létard and D. Chasseau, *Acta Crystallogr. Sect. B Struct. Sci.*, 2003, **59**, 479–486.
82 M. a Halcrow, *Chem. Soc. Rev.*, 2011, **40**, 4119.
83 G. A. Craig, O. Roubeau and G. Aromí, *Coord. Chem. Rev.*, 2014, **269**, 13–31.
84 E. Jellema, T. J. J. Sciarone, N. M. Navarrete, M. J. Hettinga, A. Meetsma and B. Hessen, *Eur. J. Inorg. Chem.*, 2011, **2011**, 91–100.
85 G. Glatz, S. Demeshko, G. Motz and R. Kempe, *Eur. J. Inorg. Chem.*, 2009, **2009**, 1385–1392.
86 R. A. Andersen, K. Faegri, J. C. Green, A. Haaland, M. F. Lappert, W. P. Leung and K. Rypdal, *Inorg. Chem.*, 1988, **27**, 1782–1786.
87 G. M. Sheldrick, *Acta Crystallogr. Sect. A Found. Crystallogr.*, 2008, **64**, 112–22.
88 G. M. Sheldrick, *Acta Crystallogr. Sect. C Struct. Chem.*, 2015, 71, 3–8
89 L. J. Farrugia, *J. Appl. Crystallogr.*, 1999, **32**, 837–838.
90 C. B. Hübschle, G. M. Sheldrick and B. Dittrich, *J. Appl. Crystallogr.*, 2011, **44**, 1281–1284.